PCCP

Accepted Manuscript

ROYAL SOCIETY OF CHEMISTRY

www.rsc.org/pccp

A TDDFT/MMPol/PCM model for the simulation of Exciton-Coupled Circular Dichroism spectra

Sandro Jurinovich,* Gennaro Pescitelli, Lorenzo Di Bari, Benedetta Mennucci*

Dipartimento di Chimica e Chimica Industriale, University of Pisa, Via Risorgimento 35, I-56126 Pisa, Italy

Abstract

We present a quantum-mechanical excitonic model to compute CD spectra of multichromophoric compounds. All the quantities needed to build the excitonic Hamiltonian are obtained through QM calculations in which the interactions among the chromophoric units are described in terms of full transition densities instead of reverting to the common dipole-dipole approximation. Environmental effects due to solvation and the perturbation due to other surrounding units are included in a self consistent way using a polarizable continuum model and a polarizable MM approach, respectively. The applications to two different coordination compounds show that the method not only successfully reproduces the experimental spectra but it can also be used to investigate the dissect the role of the various effects contributing to the final result, such as intra-molecular coupling terms and environment effects. This method can therefore represent an *ab initio*-alternative to the widely applied matrix-based approach, and in principle it has the advantage of not requiring the knowledge of any experimental data *a priori* or the transitions dipole parameters.

* Corresponding authors, e-mail: sandro.jurinovich@for.unipi.it, benedetta.mennucci@unipi.it

1. Introduction

The numerous applications of time-dependent density functional theory (TDDFT) reported in the recent years clearly show that such a method can allow the prediction of the UV-Vis absorption and circular dichroism (CD) spectra of organic and organometallic compounds with a very favorable accuracy/cost ratio especially for low-energy and local excitations.[1–5] This computational efficiency combined to ease of use has made TDDFT one of the popular quantum-mechanical (QM) approaches to study electronic spectra of molecular systems. When moving to molecular aggregates or multichromophoric systems instead, the accurate description of electronic excitations and of the related CD spectra still constitutes a challenge for quantum mechanical methods, including TDDFT.[6–8] To circumvent such increased difficulty as well as the high computational cost generally involved in the treatment of large systems, models based on the interactions of subsystems according to an exciton picture have been developed.[9–12] In particular, the recent extensions of the subsystem formulation of TDDFT within the frozen-density embedding framework[13] have shown to be an effective approach to simulate CD spectra in supramolecular systems.[14]

In the simplest exciton scheme, a pair of degenerate chromophores interacts to give a set of two non-degenerate excitonic states in the coupled system.[15] The resulting splitting mainly depends on the strength of the coupling between the chromophores' transitions. In the electronic CD spectra these exciton coupled (EC) transitions display oppositely signed peaks in the same spectral region where the absorption occurs. The resulting Cotton effects are directly related to the reciprocal orientation of the electric dipole transition moments, i.e. to the absolute molecular stereochemistry, so exciton-coupled circular dichroism (ECCD) is widely employed for non empirical assignment of the absolute configuration of organic molecules.[16,17]

In the QM description of exciton-coupled systems, the excited states are expressed as a superposition of the states of the single chromophoric units. Physically this means that in the coupled system an electronic transition is "shared" between two or more chromophores. The new excitonic transition energies and dipoles, as well as the rotational strengths determining the CD spectrum, can be calculated using the transition energies of the single units, also called "site energies", the corresponding electric dipole transition moments, and the electronic couplings between them. As an alternative to this QM exciton description, a classical method, known as DeVoe polarization model,[18,19] was developed to interpret the experimental CD spectra of the EC systems. Calculation of the CD spectrum within the DeVoe model requires

both geometrical and spectroscopic parameters. The geometrical data can be obtained once a molecular structure has been determined experimentally (by NMR spectroscopy, for instance) or theoretically (by molecular mechanics or QM calculations). The spectroscopic parameters are generally taken from the spectral properties of the chromophores, which constitute the overall molecular aggregate. Finally, a matrix-based approach is used to simulate the excitonic spectra assuming a point dipole-dipole interaction among the units.[17,20,21]

In this paper we present a revised version of the QM excitonic model which is *parameter-free* being based on the TDDFT calculation of all the necessary properties to simulate the EC spectra for coupled systems. In particular, the couplings are computed from the interaction of the full QM electronic transition densities[22,23] and not from the point-dipole approximation which is still commonly, although not exclusively,[9–14] employed in other excitonic models. Moreover, environment effects are also included in the QM calculations using a mixed continuum/atomistic classical approach in which the QM and the two classical descriptions mutually polarize.[24]

As applications of the model which from now on will be indicated as QM-EC, we have investigated three systems of increasing complexity, based on the binaphthol (1,1'-bi-2-naphthol) motif, starting from a simple derivative of the parent compound, then moving to two multi-chromophoric octahedral metal complexes. In the latter systems the metal centre is coordinated with three binaphtholate units which act as di-anionic bidentate ligands.

2. Methods

2.1 Computing the excitonic transition energies

When exciton coupling occurs between two or more interacting chromophoric units (either separate molecules or fragments of the same molecular system), the excitonic state φ_k can be described as a linear combination of the excited states η_i localized on the chromophoric units: $\varphi_k = \sum_i c_i^{(k)} \eta_i$. The expansion of φ on the η-basis allows one to find the eigenvalues and eigenfunctions by diagonalizing the corresponding exciton $\boldsymbol{H}$ matrix:

$$\boldsymbol{H} = \begin{bmatrix} H_{11} & \cdots & H_{1j} \\ \vdots & \ddots & \vdots \\ H_{j1} & \cdots & H_{ij} \end{bmatrix} \quad (1)$$

The diagonal elements $H_{ii} = \langle \eta_i | \widehat{\mathcal{H}}_{el} | \eta_i \rangle$ represent the site energies of the various units whereas the off-diagonal elements $H_{ij} = \langle \eta_i | \widehat{\mathcal{H}}_{el} | \eta_j \rangle$ represent the interaction between units

and they are generally indicated as "electronic couplings" V_{ij}. In the simplest case of exciton coupling, when a pair of two degenerate chromophores interact through a V_{12} coupling term, the two non-degenerate excitonic states are split by a quantity $\Delta E = 2V_{12}$, the so-called *Davydov splitting*.[25]

All the components of the $\boldsymbol{H}$ matrix are here obtained at TDDFT level using a fully polarizable QM/discrete/continuum method[24] to include the effects of the environment. In particular, the continuum solvation model adopted is the Polarizable Continuum Model (PCM)[26] in which the QM solute is placed into a molecule-shaped cavity surrounded by a continuum dielectric medium characterized by a static (ε) and an optical (ε_∞) permittivity. The QM solute induces a polarization of the solvent represented in terms of a set of induced charges placed on the cavity surface which act back on the QM solute, so a self-consistent approach is needed to solve the QM/PCM problem and compute the energy and the properties of the solvated system.

PCM is here combined with a discrete description of the environment based on a polarizable molecular mechanics (MM) model, in which classical point charges and induced dipoles, defined in terms of isotropic atomic polarizabilities, are used to describe the molecules of the environment.[22] The simultaneous inclusion of PCM and MMPol into the molecular Hamiltonian leads to additional perturbation terms, arising from the interaction among quantum and classical parts that can be schematized as follows:[24]

$$\hat{H}^{env} = \hat{H}^{ele}_{QM/MM} + \hat{H}_{QM/PCM} + \hat{H}^{pol}_{QM/MM} + \hat{H}_{MM/PCM} + \hat{H}^{pol}_{MM/MM} \quad (2)$$

The first three terms represent the interaction of the QM charge density with the MM charges, the PCM charges and the induced dipoles, respectively, whereas the latter two terms describe the interactions of the MM charges with the PCM charges and the induced dipoles (the interaction among MM charges is a constant term which does depend on the QM part of the system). By using the Hamiltonian reported in eq.(2) we can calculate both ground and excited states processes. In particular, in this work we applied the TDDFT linear response scheme to obtain both the site energies and the couplings in the presence of a polarizable environment.[27,23] In the calculation of both sets of properties, possible delays in the response of the environment, which correspond to a non-equilibrium solvation regime, are also taken into account.[26]

More in detail, the electronic coupling between two monomeric units *i* and *j* is calculated from the transition densities of the non-interacting units. In the case of "in vacuo" system, the coupling is composed of three terms: V_{cou}, V_{xc} and V_{ovlp} that are referred to as Coulomb,

exchange-correlation and overlap coupling terms, respectively. The Coulomb term is generally dominant with respect to the other ones and has a physical correspondence with the classical point-dipole/point-dipole interaction term[28] where the electronic transition dipole moments appear instead of the transition densities matrices $\tilde{\rho}_j\ (\boldsymbol{r}')$; namely we have:

$$V_{Coul} = \int d\vec{\boldsymbol{r}}\, d\vec{\boldsymbol{r}}'\, \tilde{\rho}_i^{\dagger}(\vec{\boldsymbol{r}}) \frac{1}{|\vec{\boldsymbol{r}} - \vec{\boldsymbol{r}}'|} \tilde{\rho}_j\ (\vec{\boldsymbol{r}}') \tag{3}$$

where the integral is performed using the standard numerical integration methods used in DFT.

It has been observed that transition density methods give more accurate results for coupling terms than the simple point-dipole approximation, especially when the interacting units are placed at short distances.[29,30]

The environment effects on the couplings are included through two additional terms, V_{PCM} and V_{MMPol}, which describe the interaction between the transition density of the unit i with the PCM charges/MMPol dipoles induced by the other unit j.[23,22]

$$V_{PCM} = -\sum_t \left[\int d\vec{\boldsymbol{r}} \tilde{\rho}_i^{\dagger}(\vec{\boldsymbol{r}}) \frac{1}{|\vec{\boldsymbol{r}} - \vec{\boldsymbol{r}}_t|} \right] q_t(\tilde{\rho}_j) \tag{4}$$

$$V_{MMPol} = -\sum_p \left[\int d\vec{\boldsymbol{r}} \tilde{\rho}_i^{\dagger}(\vec{\boldsymbol{r}}) \frac{\vec{\boldsymbol{r}}_p - \vec{\boldsymbol{r}}}{|\vec{\boldsymbol{r}}_p - \vec{\boldsymbol{r}}|^3} \right] \cdot \vec{\boldsymbol{\mu}}_p(\tilde{\rho}_j) \tag{5}$$

In most cases V_{PCM} and V_{MMPol} act as screening terms leading to a reduction of the total coupling, however, there can be specific combinations of type of excitation and orientation/distance of the interacting units which can lead to an enhancement of the total coupling.

2.2 Computing the rotational strength

The calculation of the rotational strength R determining the CD spectra is here performed following an approximate method based on the electric transition dipole moments. The rotational strength of the electronic transition $k \longleftarrow 0$, R^k, is defined as the imaginary part of the scalar product of the electric and magnetic dipole transition moments:

$$R^k = \Im m\{\langle 0|\hat{\boldsymbol{\mu}}|k\rangle \cdot \langle k|\hat{\boldsymbol{m}}|0\rangle\}$$

To account for the problem of the origin-dependence of the magnetic dipole, we can introduce the dipole-velocity formulation and exploit the correspondence of the magnetic and electric operators so to obtain a simplified formulation of R^k where only the electric transition dipole moment operators appear, namely:

$$R^k = \frac{\pi}{2\lambda_k} \sum_{i,j=1}^{N} \vec{R}_{ij} \cdot \langle 0 | \hat{\boldsymbol{\mu}}_i \times \hat{\boldsymbol{\mu}}_j | \psi_k \rangle \quad (6)$$

Where $\vec{R}_{ij}$ is the vector distance between the chromophores *i* and *j* and λ_k is the wavelength of the excitonic electronic transition $k \longleftarrow 0$. The generalization of eq.(6) to an excitonic system yields:[31,32]

$$R^k = \frac{\pi}{2\lambda_k} \sum_{i,j=1}^{N} c_i^{(k)} c_j^{(k)} \vec{\boldsymbol{R}}_{ij} \cdot \vec{\boldsymbol{\mu}}_i \times \vec{\boldsymbol{\mu}}_j \quad (7)$$

where the $c_i^{(k)}$ coefficients in eq.(6) are the eigenvectors coming from the diagonalization of the excitonic matrix in eq.(1). To finally obtain the CD spectra, excitonic energies and rotational strengths are combined with normalized Gaussian line shape functions, namely:

$$\Delta\varepsilon(\tilde{\nu}) = \frac{1}{2.296 \times 10^{-39} \Gamma_k \sqrt{\pi}} \sum_{k=1}^{N} R^k \tilde{\nu}_k e^{-\left(\frac{\tilde{\nu}-\tilde{\nu}_k}{\Gamma_k}\right)^2} \quad (8)$$

where the rotational strengths are expressed in cgs units and $\tilde{\nu}$ is in cm^{-1}. As the line–shape function should phenomenologically account for the fact that experimental bands are very different from the infinitely sharp ones predicted by a theoretical approach neglecting roto-vibrational structure, collisional dynamics, and various types of broadening mechanisms, the Γ parameters, which are defined as half the bandwidth at $1/e$ peak height, were set so to reproduce the experimental bandwidths.

The absorption spectrum lineshape is obtained following a similar procedure explained for CD where the excitonic dipole strengths are expressed as the combination of the expansion coefficients and the transition dipole moments of the unperturbed chromophores.

2.3 Computational details

The full computational strategy used to obtain the EC spectra can be summarized in the workflow illustrated in Figure 1. We first extract the geometry of the monomeric units starting from an input geometry of the full system, such as crystallographic data, NMR optimized structures or computationally optimized geometries.

Once defined the monomeric units, the computational approach can be roughly divided into three main steps: i) calculation of the site energies of each unit; ii) calculation of the couplings between all pairs; iii) combination of the data obtained in i) and ii) to form the excitonic Hamiltonian which is then diagonalized. Once all monomeric data are collected, one can decide to select only some specific transitions of interest in each monomeric unit to build the

excitonic Hamiltonian. This selection can be very useful to decompose the EC spectra into different contributions coming from different interactions.

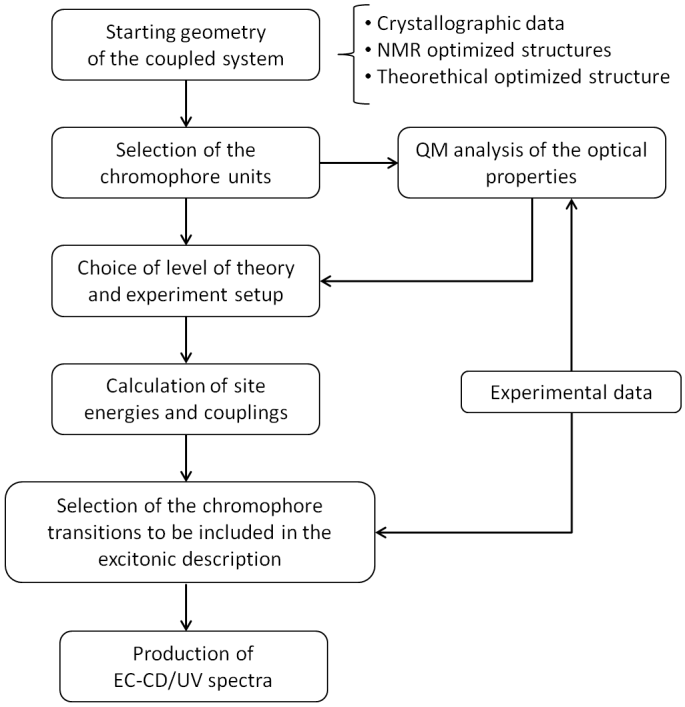

Figure 1.Workflow to simulate the excitonic spectra.

All the calculations have been performed with a locally modified version of the Gaussian09 suite of programs.[33] A specific computational tool has been developed to construct the excitonic Hamiltonian from the Gaussian output, diagonalize it and produce the EC spectra.[34]

The ground state geometries of all systems have been optimized in the proper solvent using M062X/6-31+G(d,p)/PCM level of theory.[35,26] Site energies, transition densities and couplings have been computed at TDDFT level using the cam-B3LYP functional.[36] For isolated monomeric units also a SAC-CI calculations were performed as a benchmark.[37]

Environmental effects have been included using the combined MMPol/PCM approach described above. In particular, the effects induced by the atoms of the system not involved in the electronic transition have been represented by a set of classical point charges and induced dipoles through the MMPol approach.[22] Charges were determined with the *Merz-Singh-Kollman* method[38,39], at the same level of theory of the TDDFT calculations and for isotropic atomic polarizabilities the experimental values were used.[40] The PCM in its IEFPCM version[26] has instead been used to include the effect of the solvent. Cavities were built using the united atom topological model and the IEFPCM calculations were performed with G03default option.

3. Results and Discussion

3.1. 1,1'- Binaphthyl compound

The 1,1'-binaphthyl scaffold is found in a manifold of chiral ligands for enantioselective catalysis and molecular recognition.[41,42] As it is well known, the 1,1' linkage provides long lived atropisomers,[43] while at the same time ensuring a wide conformational freedom of the 2,1,1',2' dihedral angle. Consequently, binaphthyls bearing donor atoms or groups at the 2 and 2' positions act as powerful chelators, easily accommodating practically all metal ions, with different geometries and binding modes.[42] Comparative experimental and theoretical studies of conformationally-locked (or at least biased) compounds have revealed that chiroptical properties are highly angle-dependent and that in principle there are conformations possibly leading to oppositely signed spectra.[44,45] Quantitative correlations between chiroptical properties and conformations of enantiopure derivatives of 1,1'-binaphtyl have been deeply investigated with the application of DeVoe polarizability model[45–47] and recently also with high-level wave function-based QM methods.[48,49]

In order to test the QM-EC model, we focused on (S)-3,5-dioxa-cyclohepta[2,1-a;3-4-a'] dinaphtalene (dioxepine) (see Figure 2). In this 1,1'-binaphthyl compound the degree of freedom involving the dihedral angle ϑ between C1-C2-C1'-C2' is removed because 2 and 2' oxygen atoms are linked to the same methylene group.

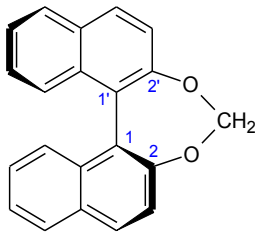

Figure 2. Molecular structure of (S)-dioxepine.

The (S)-dioxepine geometry was optimized under a C_2 symmetry constraint and the resulting structure showed a ϑ dihedral angle of 48.6°. The chromophoric unit was obtained by cutting the C1-C1' and the O-CH_2 bonds, then the vacant valence was saturated with hydrogen atoms to obtain the 2-naphtol (NpOH) structure.

The calculated NpOH absorption spectra revealed the typical bands of the 2-substituted naphthalene compound: two weak peaks in the low energy region of the spectrum (330-280 nm) together with an intense peak at higher energy at about 220 nm. These bands

respectively correspond to the transitions found in naphthalene and namely ^1L_b, ^1L_a, ^1B_b in the Platt's notation.[50–52]

Exciton coupling calculations are sensitive to the magnitude and the relative orientation of the transition dipole moments. Therefore a crucial role is played by the correct assignment of dipole direction and intensity of the monomer unit. The ^1L_b and ^1B_b electronic transition dipole moments are directed along the long molecular axis of the naphthalene whereas the ^1L_a is perpendicular to it, but the presence of substituents in the naphthalene moiety can strongly perturbs this picture depending on their nature and position: this perturbation is expected to be significant true here owing to the extension of conjugation brought about by the 2-hydroxy or its anionic form.[53]

In Table 1 we report the excited state properties of NpOH computed in vacuo and in THF for the three main transitions using different computational levels. All the calculated spectra compare well with previous calculations and the experimental spectrum of NpOH.[54–56]

		VACUO				THF			
		E(eV)	**E** (nm)	$\|\mu\|^2$(D^2)	ϑ (deg)	**E** (eV)	**E** (nm)	μ^2(D^2)	ϑ (deg)
SAC-CI 6-311+G(d,p)	^1L_b	4.118	300	2.7	**-76**				
	^1L_a	4.533	273	5.3	**89**				
	^1B_b	6.065	204	18.9	**1**				
cam-B3LYP 6-31G(d)	^1L_b	4.602	269	3.4	**-65**	4.582	271	4.5	**-70**
	^1L_a	4.811	258	3.9	**88**	4.795	259	4.2	**85**
	^1B_b	6.180	201	18.0	**5**	5.968	208	20.4	**4**
cam-B3LYP 6-31+G(d)	^1L_b	4.530	274	3.5	**-72**	4.508	275	4.8	**-77**
	^1L_a	4.730	262	3.9	**86**	4.712	263	4.2	**84**
	^1B_b	5.990	207	17.1	**3**	5.765	215	21.2	**2**
cam-B3LYP 6-311+G(d)	^1L_b	4.501	275	3.5	**-73**	4.479	277	4.7	**-78**
	^1L_a	4.694	264	3.8	**87**	4.679	265	4.1	**86**
	^1B_b	5.964	208	16.9	**3**	5.738	216	21.1	**2**
Experimental[a]	^1L_b	3.78 [b]	328	1.45					
	^1L_a	4.36 [b]	284	4.85					
	^1B_b	5.53	224	50.0					

Table 1. TD bright excited states of NpOH computed at different levels of theory. The rotation angle of the transition dipole moments is referred to the long axis of NpOH unit. (*a*) In isooctane[54], (*b*) 0-0 band.

More in details, TD cam-B3LYP overestimates the SAC-CI transition energies but it correctly reproduces orientations and absolute values of the transition dipole moments. Larger basis sets for TD cam-B3LYP only provide a small red-shift of all the excited state energies but they

do not significantly affect the transition dipole moments. The inclusion of a polarizable environment (here mimicking the THF solvent) affects only the position of the ^1B_b transition which is shifted by -0.2 eV, and, as expected, the solvent enhances the magnitude of transition dipole moments.

The experimental CD spectrum of dioxepine is dominated by the intense Cotton effects due to the high energy π-π^* ^1B_b transition. The calculated ^1B_b couplings are reported in Table 2 for gas-phase and solvated systems.

		VACUO		PCM (Tetrahydrofuran)		
		QM-V_{12}	F-V_{12}	QM-V_{12} TOT	QM-V_{12} PCM	F-V_{12}
cam-B3LYP	6-31G(d)	**1143**	1944	**918**	-425	1125
	6-31+G(d)	**1159**	1634	**903**	-421	1036

Table 2. ^1B_b coupling values (QM-V_{12}); for the in solution calculations the PCM contribution is also shown. F-V_{12} refers to the point-dipole couplings (which in THF have been screened by the Forster factor n^2=1.974). All values are in cm^{-1}.

As expected from the previous analysis on the transition dipole moments, also for the couplings no relevant differences are found by enlarging the basis set. To be noted that, if a point-dipole approximation is used, the couplings (F-V_{12}) are largely overestimated showing the importance of a proper description based on a full transition density. Such an overestimation is also found in a previous estimate (1560 cm^{-1}) obtained still adopting the point-dipole approximation but with experimentally derived transition dipoles.[17] From Table 1 we have seen that the inclusion of the solvent effects enhances the magnitude of the transition dipole, but here we see that it also screens the interactions between the monomer units leading to a reduction of ca. 20% of the final coupling.

The simulated excitonic absorption and CD spectra for dioxepine are reported in Figure 3 for both gas-phase and solvated systems. In the same figure we also report the spectra obtained from a TDDFT calculation on the whole dioxepine system.

As evident from both graphs, the excitonic and the full calculations are in general good agreement though in the former we observe a larger separation between the excitonic energies. In addition, a weak positive band is found in the long-wavelength side of the CD spectrum obtained with the full TDDFT calculations, which is not present in the excitonic one.

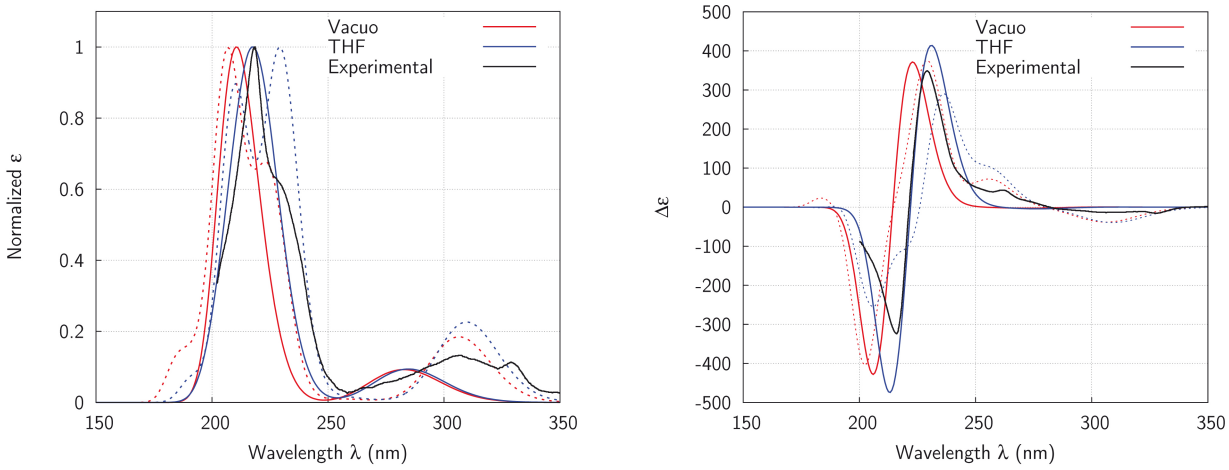

Figure 3. EC absorption (left) and CD (right) spectrum simulated at cam-B3LYP/6-31+G(d) level of theory. Solid lines are referred to the excitonic calculation; dotted lines are referred to the TD calculation on the entire dioxepine system at the same level of theory. The experimental spectra are also reported in black.[46] The computed spectra are shifted in such a way that the ^1B_b excitonic band in THF matches with the experimental one.

This band, which is also detectable in the experimental spectrum, has been assigned to a inter-naphthalene charge-transfer transition which is made possible by the relatively small dihedral angle of the dioxepine.[57] From our calculations, the involved orbitals are indeed delocalized on the full system (see Figure S1 in the Supporting Information) and this explains why such a band is not reproduced in the excitonic model. The excitonic spectra are however in good agreement with the experimental data for what concerns the modeling of the ^1B_b couplet. In general, no appreciable differences are found between gas-phase and solution, except for the red-shift of ^1B_b couplet which reflects the trend of the monomer site energies.

3.2 Transition metal compounds

We move now to investigate the optical properties of two complexes, where three 2,2'dihydroxy-1,1'-binaphtyl (BINOL) units chelate a lanthanide ion. We chose these two systems, as they are both endowed with a D_3 symmetry but they present a profoundly different organization of the naphthalene moieties. In both cases, geometrical structures in solution are available from paramagnetic NMR measurements.

3.2.1 $Na_3Yb(BINOLate)_3$

The first system is a heterobimetallic complex, obtained by reaction of an alkali metal salt (M^+) of BINOL typically with a lanthanide triflate (or chloride). The resulting complexes obtained from enantiopure BINOLate, have formula $M_3[Ln(BINOLate)_3]$ (M=Li,Na,K;

Ln=Yb,Lu) and share very similar XRD structures, with each M^+ bridging two BINOLate units through a O-M-O linkage.[58,59] The solution structure of $Na_3[Yb((S)\text{-BINOLate})_3]$ was studied in detail and it displays the six oxygen atoms at the corners of an almost perfect trigonal antiprism (a somewhat compressed octahedron), held rigidly in place by Yb^{3+} coordination and through the O-Na-O bridges.[60] Starting from this structure,[60] we extracted and optimized a BINOL unit maintaining the ϑ angle fixed at 76.7°. Then we reconstructed the tridimensional structure of the complex superimposing the optimized C_2 symmetric BINOL on the starting structure and minimizing the RMSD between C and O atoms. This procedure did not alter the tridimensional structure but allowed the chromophore geometries to relax. The obtained structure is reported in Figure 4 and shows a D_3 symmetry.

The absorption spectrum of $Na_3Yb(BINOLate)_3$ is dominated by the π-π* transition of the aromatic chromophore in the 200-400 nm range. Experimental UV-Vis and UV-ECD spectra of $Na_3Yb(BINOLate)_3$ and analogue lanthanide compounds do not reveal detectable transitions involving the metal center. According to the DeVoe calculations already performed on this system,[61] we identified the monomer chromophoric unit as 2-naphtoate (NpO^-) and its geometry was extracted from the symmetric structure of Figure 4 following the same procedure explained before for dioxepine.

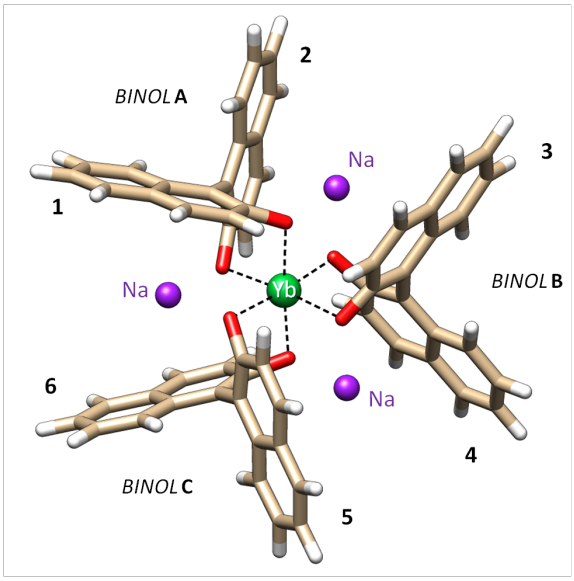

Figure 4. $Na_3Yb(BINOLate)_3$ structure used for the excitonic calculation. The complex is formed by 3 BINOL units (A, B and C), that coordinate the Yb^{3+} central metal cation through their deprotonated oxygen donor atoms. The position of Na^+ is extrapolated from the solid-state X-ray structure.

The monomer unit is negatively charged and the absorption spectrum shows some differences with respect to the neutral NpOH monomer.[61] The simulated absorption spectrum is reported in Figure 5 together with the experimental one.

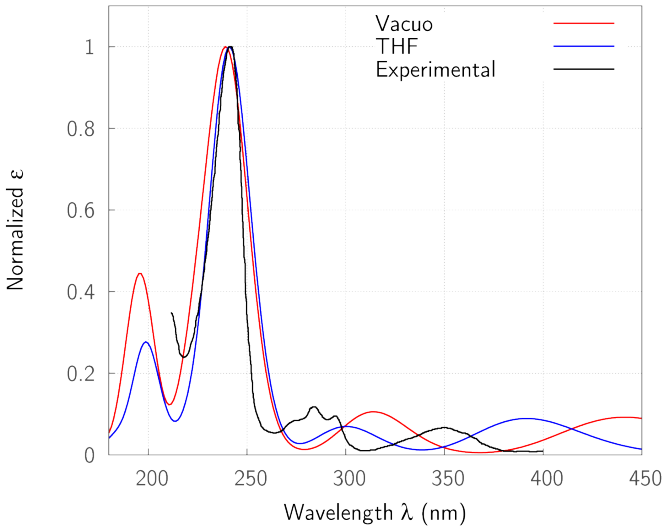

Figure 5. TD cam-B3LYP/6-31G(d) absorption spectra of NpO^- computed in vacuo and in water, compared with the experimental UV-Vis spectrum of 2-naphtol in aqueous NaOH.[60] The computed spectra are shifted in such a way that the ^1B_b band matches with the experimental one.

Since no significant differences were found in terms of relative position of the transition energies for different basis sets (see Table S1 in the Supporting Information), the cam-B3LYP/6-31G(d) level of theory has been adopted for the excitonic calculations allowing us to save computational time both for the site energies calculation (6 chromophores) and for couplings between all the possible chromophore pairs (15 couplings in total).

By comparing the spectra with that of the neutral NpOH (summarized in Table 1 above), some differences appear: the ^1L transitions are separated by about 1 eV and a further high energy transition, namely ^1B_a, appears in the region < 200 nm with an intensity of about 50-70% with respect to the most intense ^1B_b transition. The orientation of the transition dipole moments is different from that of the neutral NpOH, due the presence of the O^- instead of the OH which has a strong influence on the excited state properties, and the dipole of the ^1B_b transition is further rotated by ~ 20° in the direction of the substituent with respect to the NpOH (see Table S1 in the Supporting Information). Also the ^1L_a and ^1L_b transition dipoles are significantly changed passing from NpOH to NpO^-. If we look at the relative peak positions, the lower energies bands are both red-shifted with respect to the position of the most intense ^1B_b. The experimental UV-Vis spectrum was truncated at 210 nm so we could not exactly compare

the position and the intensity of the high energy ^1B_a band. However the calculated energy difference between ^1B_b and ^1B_a seems to be overestimated with respect to the experimental data and this will have some consequences in the following excitonic description.

Before performing the EC calculation on the whole complex, we computed the in vacuo CD spectrum of a BINOLate unit extracted from the $Na_3Yb(BINOLate)_3$ structure and we compared the results with the excitonic ones at the same level of theory, considering only two bonded NpO^- monomer units (e.g. units 1-2 of BINOLate A). In EC-CD calculations, the first four π-π* bands for each NpO^- unit were included. The two calculated EC-CD spectra, reported in Figure 6, are in remarkably good agreement and the excitonic calculation also reproduces the asymmetry found for ^1B_b band due to the coupling between the two high energy transitions.

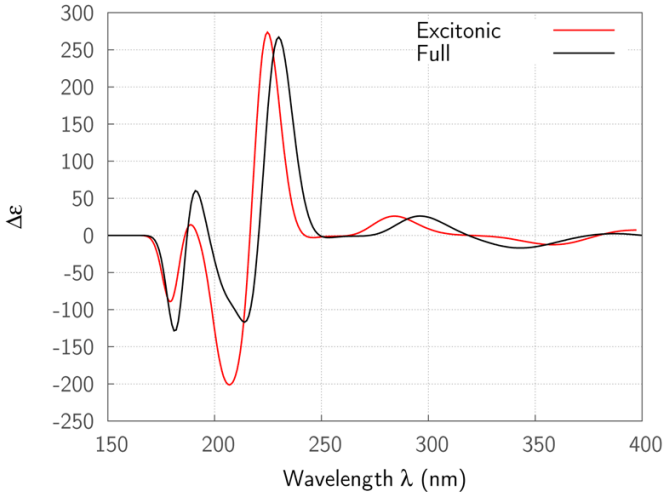

Figure 6. CD spectrum of BINOLate computed at cam-B3LYP/6-31G(d) level of theory, in vacuo, in the geometry adopted in $Na_3Yb(BINOLate)_3$ structure. The black line refers to the TD calculation performed on the entire BINOLate system, red line is the EC-CD spectrum.

The following EC analysis is instead performed including all six monomeric units. In vacuo calculations were performed on all possible NpO^- isolated pairs, neglecting the cations present in the $Na_3Yb(BINOLate)_3$ structure. In a more realistic picture we considered each monomer perturbed by the presence of the other NpO units, which were modeled at MMPol level, and the whole system was surrounded by a continuum solvent. The MMpol part of the system also included the Na^+ metal ions and/or the Yb^{3+} modeled as screened partial charges of 0.5 and 1.5 respectively. In the following discussion we will refer to the different models used as summarized in the following scheme:

	QM	MMPol	PCM
Vacuo	NpO monomer	none	none
MMPol(Na)/PCM	NpO monomer	Other NpO units, Na (0.5)	THF
MMPol(Na-Yb)/PCM	NpO monomer	Other NpO units, Na (0.5), Yb (1.5)	THF

The UV excitonic spectra calculated with the different models are reported in Figure 7 together with the experimental one measured in THF.

From the spectra reported in the figure, we can see that the different descriptions of the environment strongly influence the position of the two low-energy bands. The inclusion of the central Yb charge leads to better results for what concerns the position of the ^1L_a and ^1L_b peaks. The two high-energy bands do not seem to be strongly perturbed by the different environmental descriptions. This is in accord with the classical notion that the stronger is an electronic transition, the less it will be perturbed by secondary factors such as substituents.

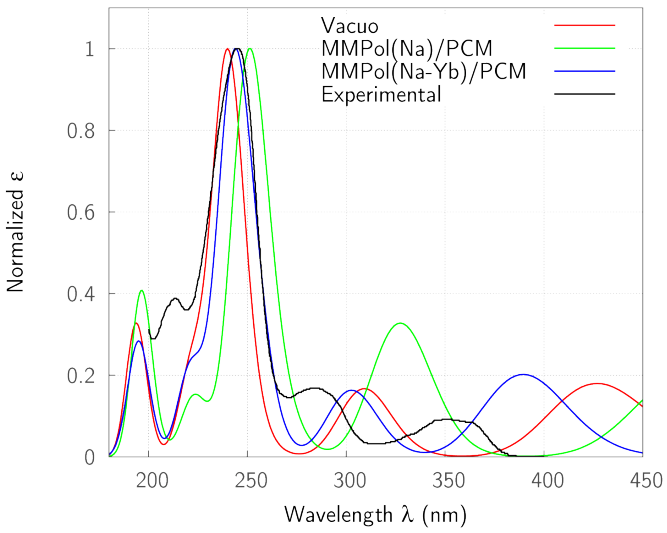

Figure 7. EC absorption spectra computed at cam-B3LYP/6-31G(d) level of theory. The experimental $Na_3[Yb((S)\text{-}BINOL)_3]$ absorption spectrum in THF is reported in black.[60] The computed spectra are shifted in such a way that the ^1B_b excitonic band at MMPol(Na-Yb)/PCM level matches with the experimental one.

The experimental shoulder at 215 nm, if compared with the experimental CD spectrum, may be assigned to the ^1B_a transition, even if no experimental data are available in the region < 200 nm. In this case, as already discussed for the monomer spectrum, the two simulated high-energy excitonic bands are more separated in energy with respect to the experimental data. Due to the D_3 symmetry, the six NpO monomers have the same site energies and the couplings

can be divided into two groups, characterized by different distances and relative orientations of the units. V_{12}, V_{34}, V_{56} refer to the *intra*-molecular coupling between two adjacent units chemically bonded to each other; the other terms refer instead to *inter*-molecular couplings between units that belong to different BINOLate groups. The computed EC-CD spectra are reported in Figure 8 for the gas-phase and the solvated systems.

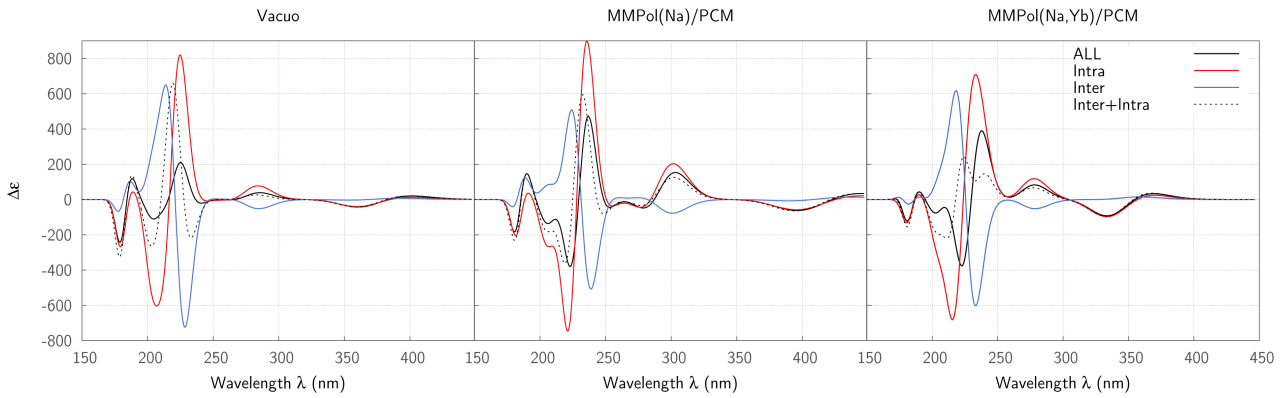

Figure 8. EC-CD $Yb(BINOL)_3$ spectrum simulated at cam-B3LYP/6-31g(d) level of theory with different environmental descriptions.

In particular, each graph compares the EC-CD spectrum computed by considering all possible coupling terms (black lines) with the two spectra calculated taking into account only the *intra*-molecular (red lines) and *inter*-molecular (blu lines) couplings, respectively. Moreover, a further "sum" spectrum is also reported: this is obtained by simply adding the *intra* and *inter* spectra (black dotted lines).

In all environments, the *inter* and *intra* spectra show an opposite sign in almost all the specral regions and the intensities of the *intra* spectrum are always higher: this indicates that the *intra*-interactions have the major contribution to the total CD spectrum. This is the same result previously reached by means of DeVoe calculations.[61] When we compare the results from the present treatment with those obtained thorough DeVoe calculations, we have to recall that the in these latter ones experimentally-derived parameters such as transition frequencies and intensities were used.[20] In the current treatment, instead, both frequencies and intensities are computed *ab initio*, and only the band-width is arbitrarily chosen on a best-fitting basis.

The environment effects alter the shape of the CD spectrum, especially when the central ion is included in the calculations, but in general they do not affect the sign of the strongest

excitonic bands. In Figure 9 we compare the EC-CD spectra obtained within the MMPol(Na-Yb)/PCM scheme with the experimental one.

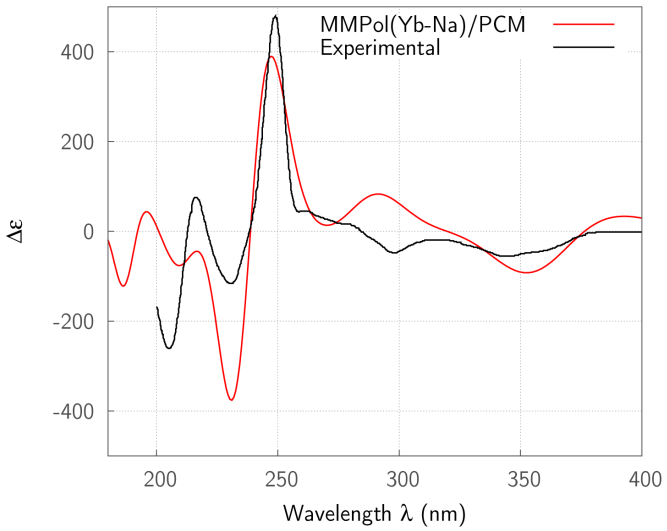

Figure 9. EC-CD Yb(BINOL)$_3$ spectrum simulated at cam-B3LYP/6-31g(d) level of theory with the MMPol(Yb-Na)/PCM environmental description (blue line) compared with the experimental data (black line). The computed spectra are shifted in such a way that the ^1B_b excitonic band matches with the experimental one.

In the region of ^1B_b and ^1B_a couplings the excitonic results are in agreement with the experimental data for what concerns the sign of the excitonic bands. However, the total spectrum has lost the asymmetry in the ^1B_b and ^1B_a region, and this may be due to an overestimation of the *inter*- contribution to the total coupling, as it is possible to see comparing the spectra in Figure 8. We also note that only by including the central Yb charge the shape of the low energy spectrum > 250 nm is recovered, while in vacuo simulation gives wrong results also for the relative intensities of the two high energy couplets (see Figure 8).

We finally observe that site energies and couplings are sensitive to the value of the partial charge assigned to the cations and this affects the EC-CD simulations. Indeed, the ligand-lanthanide bond in this kind of complexes is known to be of almost purely electrostatic nature.[61] Moreover, the position of the Na^+ cations was obtained from the solid-state data of $Na_3Yb(BINOLate)_3$ crystals which is clearly a not very reliable description for the solvated system.

3.2.2 Yb(BINOLAM)$_3$

The second set of Ln^{3+} complexes was obtained by using (S)-3,3'-bis(diethylaminomethyl)-1-1'-bi-2-naphtol, known as BINOLAM, as the chiral ligand. In particular, we focused on the Yb(BINOLAM)$_3$ complex (see Figure 10) .[62]

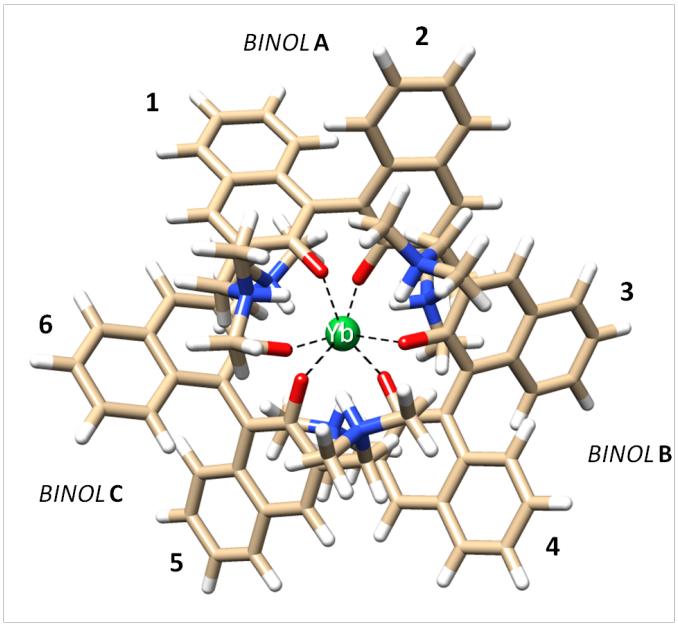

Figure 10. $Yb(BINOLAM)_3$ structure obtained by superimposing the BINOLAM optimized structures. The complex is formed by 3 BINOLAM zwitterionic units (A, B and C) that coordinate the Yb^{3+} central metal cation thorough their deprotonated donor oxygen atoms.

The formation of this complex does not require the action of an external basis, contrary to what we have seen for$M_3Ln(BINOLate)_3$, because the diethylamino group performs this role intramolecularly, as we shall discuss below. The coordination polyhedron is rather far from the antiprism and it is better described by a twisted trigonal prism. The six naphthalenes occupy an equatorial region, which is again in contrast with $Na_3Yb(BINOLate)_3$, as one may appreciate by comparing the Figures 4 and 10, where the complexes are watched from the C_3 axis in both cases. The ϑ dihedral angle between the two aromatic rings in the free ligand BINOLAM is 90° in the crystal structure.[62] Thus, $Yb(BINOLAM)_3$ complex offered an interesting complement to the $Na_3[Yb((S)\text{-}BINOLate)_3]$ to investigate the effects of a profoundly different arrangement between three BINOLate-type ligands. The diethylaminonaphthol (deaNpOH) can be envisaged to display a strong H-bond propensity defining a 6-membered cycle as represented by the resonance hybrid between the two limit forms reported in the following scheme:

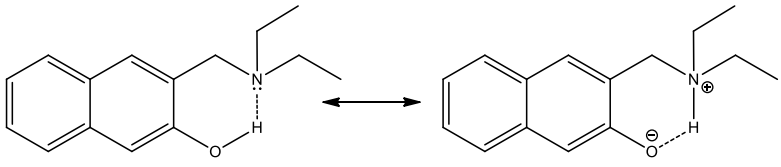

The X-ray diffraction on the BINOLAM crystals suggests that in the neutral ligand the hydroxyl group is an H-bond donor, increasing the amount of negative charge on the oxygen. However, when BINOLAM coordinates Yb, some structural rearrangements occur: i) the dihedral angle ϑ varies because of the coordination structural effect in the octahedral arrangement, passing from 90° in the free ligand crystal to 63° in solution; ii) the relative weight of the two limit resonance forms changes in favor of the zwitterionic one. Unfortunately the location of the hydrogen atom has not been clarified yet.[62]

In the following analysis we started from the solution structure obtained through accurate analysis of paramagnetic NMR data[62] and we modified it but preserving the dihedral ϑ angle and the relative position of the BINOLAM units. In particular, we replaced N-ethyl groups of the BINOLAM unit with methyl groups to reduce the number of atoms to treat. On such a unit we performed a geometry optimization keeping the dihedral angle between the two naphthalene ring fixed and imposing a C_2 symmetry.

In general, the position of hydroxyl hydrogen depends both on the acid-base properties of hydroxyl and amine groups and on the local environment. Here, we found that the minimum energy structure corresponded to the neutral form of the ligand, in which the hydroxyl group acts as H-bond donor (see the Figure S2 in the Supporting Information). However, we expect that when BINOLAM interacts with the Yb^{3+} metal center, the strong Lewis acidity of the lanthanide causes a proton migration onto the basic site leading to a zwitterionic structure of BINOLAM. To prove it we performed a geometry optimization of the $Yb(BINOLAM)^{3+}$ in acetonitrile using a pseudo-potential for Yb (MWB28). Starting from the neutral BINOLAM structure and freezing both the dihedral angle and the O-Yb distance, the optimization indeed converged to the zwitterionic form of BINOLAM. Thus, for the following calculations the zwitterionic form of the diethyaminonaphthol mojety was used (N-H distance fixed to 1.01 Å). The calculated absorption spectrum and electronic properties (including the orientation of the transition dipole moments) were found to be closer to the NpO^- monomer than to the neutral NpOH. The energy splitting between ^1B_b and ^1B_a site energies was about 0.3 eV smaller than in the NpO anion. As already done for $Na_3Yb(BINOLate)_3$, here we report the excitonic analysis obtained at cam-B3LYP/6-31G(d) level of theory whereas the comparison between other level of theory is reported in the Table S2 in the Supporting Information.

The three different environmental schemes for $YbBINOLAM_3$ system can be summarized as follows:

	QM	MMPol	PCM
Vacuo	NapNOmonomer	none	none
MMPol/PCM	NapNOmonomer	Other deaNpO units	acetonitrile
MMPol(Yb)/PCM	NapNOmonomer	Other deaNpO units, Yb (1.5)	acetonitrile

We simulated the EC-CD spectrum of the octahedral complex reconstructed replicating the optimized C_2 BINOLAM following the same strategy used for YbBINOL$_3$. In the EC-CD simulation we included all the excited states resulting from the TD-DFT calculations with wavelength in the range 150-450 nm. The EC absorption spectra is reported in Figure 11 for the different environments.

As shown in the reported spectra, the different environments modify the positions of the (^{1}L) low energy bands whereas the ^1B_a position is not significantly affected. We also note that the inclusion of the central metal charge enhances the ^1B_b intensities and leads to ^1L_a and ^1L_b bands closer to the ^1B_b one. This is the similar trend observed above for NpO$^-$, as it is expected because of the already noticed similarity between deaNpO and NpO$^-$ monomers.

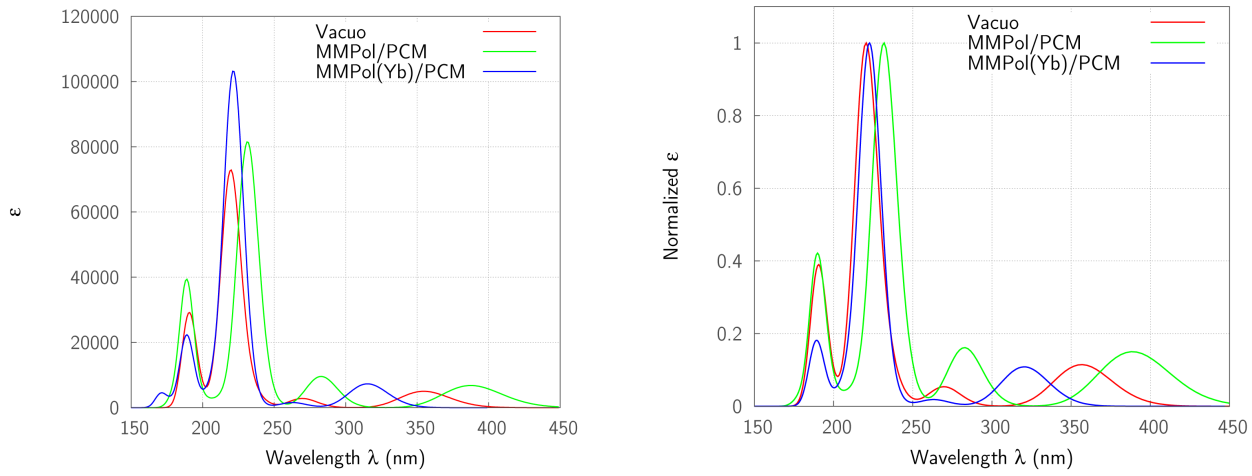

Figure 11. Absorption spectra simulated at cam-B3LYP/6-31g(d) level of theory, with different environmental description. The left picture represents the NapNO TDDFT spectra, in the right picture the normalized EC spectra are reported.

Due to the D_3 symmetry, the *inter-/intra*-chromophore analysis can be performed as previously done for $Na_3Yb(BINOLate)_3$ and the resulting excitonic spectra are reported in Figure 12.

The in vacuo EC-CD spectrum was characterized by two intense exciton couplets with comparable intensities in the region 180-250 nm region, which derived from the interaction between ^1B_b and ^1B_a transitions of the monomeric units. Passing to MMPol/PCM simulations,

the overall appearance of the high-energy couplet is modified by a different balance of the *intra*- and *inter*-contributions. When the central charge is added the EC-CD spectrum is further modified in the 200-250 nm region and the ^1B_b couplet becomes definitely more intense. The relative weight of intra/inter contributions is very sensitive to the environment and determines the general shape of the total CD spectrum (see also Figure S3 in the Supporting Information).

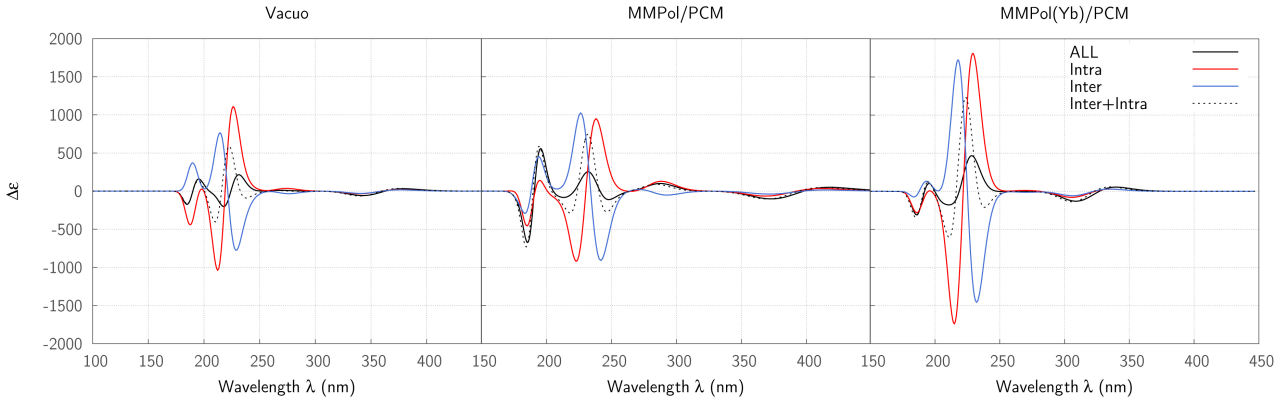

Figure 12. EC-CD Yb(BINOLAM)$_3$ spectrum simulated at cam-B3LYP/6-31g(d) level of theory with different environmental description.

If we compare the excitonic results with the experimental CD spectrum, see Figure 13, the best agreement is obtained with the MMPol(Yb)/PCM description: all observed peaks are reproduced by the simulated spectrum (except for the negative deflection on the long-wavelength side of the positive ^1B_b band). In particular, the asymmetry in the ^1B_b-^1B_a couplet is reproduced by the calculations even if its energy separation is larger than in the experimental spectrum. This could be ascribed to the overestimation in ^1B_b and ^1B_a splitting, as previously observed for the NpO monomer. The high-energy (^1B_a) region was problematic also in the previous DeVoe simulations[62].

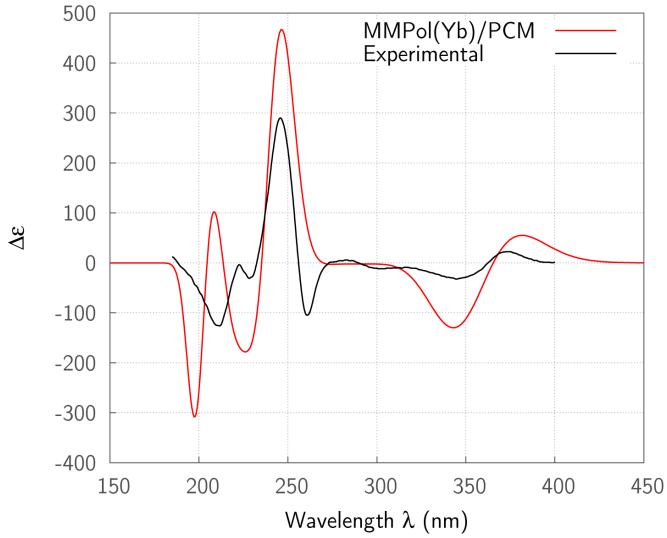

Figure 13. EC-CD Yb(BINOL)$_3$ spectrum simulated at cam-B3LYP/6-31g(d) level of theory with the MMPol(Yb)/PCM environmental description (red line) compared with the experimental data (black line) in acetonitrile.[62] The computed spectra are shifted in such a way that the ^1B_b excitonic band matches with the experimental one.

Conclusions

In this paper we have presented a full QM excitonic model to compute the absorption and CD spectra of multichromophoric chiral compounds. In such a model the interactions between the monomeric units are obtained in terms of TDDFT transition densities calculated in the presence of bulk solvation effects through PCM and the perturbation due to neighbouring units through a polarizable MM description.

A simple binaphthyl system has been first simulated to test the method, then more extended molecular systems have been deeply investigated: namely two coordination compounds, $Na_3Yb(BINOLate)_3$ and $Yb(BINOLAM)_3$, where three binaphthol units in di-anionic form coordinate a lanthanide ion. The selected compounds share the common feature of similar chromophores and environment, but provide two completely different geometries and arrangement of the naphthoates. These differences result in different excitonic spectra.

In both the investigated metal complexes, a complete description of the system has been achieved by including both the *intra*- and *inter*- binaphthyl interactions, which contributed in an opposite way to the total spectrum. In all cases, we found that the environment plays a crucial role in determining the excitonic spectra through modifications of both site energies and couplings. The best agreement with experimental data was in fact obtained in the presence of both solvation effects and the electrostatic/polarization effects due to the other monomeric units. We have also shown that the central metal ion not only plays a fundamental role in determining the geometry of the complex, but it can also affect the excited state

properties of the monomers: here we have shown that a simple but effective way to model its effect is in terms of a screened classical charge.

Even if the model presents some clear limitations, e.g. no vibronic effects are included and geometrical fluctuations are neglected, the applications here presented show that the EC-QM approach properly accounts for the main electronic and environmental effects and it can be applied to any (supra)molecular system, provided that it can be decomposed into independent, but interacting parts. In addition, our method is open to improvements, by increasing the accuracy of the calculations of monomer properties (and couplings), for example by moving from TDDFT to highly correlated QM methods. Therefore, it can represent an *ab initio*-alternative to the widely applied matrix-based approach, and in principle it has the advantage of not requiring the knowledge of any experimental data *a priori*.

Acknowledgement

S.J. and B.M. acknowledge the European Research Council (ERC) for financial support in the framework of the Starting Grant (EnLight - 277755).

Bibliography

1. S. Grimme, *Reviews in Computational Chemistry*, John Wiley & Sons, Inc., Hoboken, NJ, USA, 2004, vol. 20.
2. M. E. Casida and M. Huix-Rotllant, *Annu. Rev. Phys. Chem.*, 2012, **63**, 287–323.
3. D. Jacquemin, E. A. Perpète, I. Ciofini, and C. Adamo, *Acc. Chem. Res.*, 2009, **42**, 326–34.
4. S. S. Leang, F. Zahariev, and M. S. Gordon, *J. Chem. Phys.*, 2012, **136**, 104101.
5. C. Adamo and D. Jacquemin, *Chem. Soc. Rev.*, 2013, **42**, 845–56.
6. A. Dreuw and M. Head-Gordon, *Chem. Rev.*, 2005, **105**, 4009–37.
7. D. J. Tozer, *J. Chem. Phys.*, 2003, **119**, 12697.
8. O. Gritsenko and E. J. Baerends, *J. Chem. Phys.*, 2004, **121**, 655–60.
9. J. D. Hirst, K. Colella, and A. T. B. Gilbert, *J. Phys. Chem. B*, 2003, **107**, 11813–11819.
10. K. J. Fujimoto, *J. Chem. Phys.*, 2010, **133**, 124101.
11. M. Rudolph and J. Autschbach, *J. Phys. Chem. A*, 2011, **115**, 2635–49.

12. K. A. Kistler, C. M. Pochas, H. Yamagata, S. Matsika, and F. C. Spano, *J. Phys. Chem. B*, 2012, **116**, 77–86.

13. J. Neugebauer, *J. Chem. Phys.*, 2007, **126**, 134116-12.

14. J. Neugebauer, J. Veldstra, and F. Buda, *J. Phys. Chem. B*, 2011, **115**, 3216–25.

15. M. Kasha, H. R. Rawls, and M. Ashraf El-Bayoumi, *Pure Appl. Chem.*, 1965, **11**, 371–392.

16. N. Berova, L. Di Bari, and G. Pescitelli, *Chem. Soc. Rev.*, 2007, **36**, 914–31.

17. S. Superchi, E. Giorgio, and C. Rosini, *Chirality*, 2004, **16**, 422–51.

18. H. DeVoe, *J. Chem. Phys.*, 1964, **41**, 393-400.

19. H. DeVoe, *J. Chem. Phys.*, 1965, **43**, 3199-3208.

20. J. Grunenberg, L. Di Bari, and G. Pescitelli, in *Computational Spectroscopy*, ed. J. Grunenberg, Wiley-VCH Verlag GmbH & Co. KGaA, Weinheim, Germany, 2010.

21. N. Berova, P. L. Polavarapu, K. Nakanishi, and R. W. Woody, in *Comprehensive Chiroptical Spectroscopy: Instrumentation, Methodologies, and Theoretical Simulations, Volume 1*, eds. N. Berova, P. L. Polavarapu, and R. W. Woody, John Wiley & Sons, Inc., Hoboken, NJ, USA, 2012.

22. C. Curutchet, A. Muñoz-Losa, S. Monti, J. Kongsted, G. D. Scholes, and B. Mennucci, *J. Chem. Theory Comput.*, 2009, **5**, 1838–1848.

23. M. F. Iozzi, B. Mennucci, J. Tomasi, and R. Cammi, *J. Chem. Phys.*, 2004, **120**, 7029–40.

24. S. Caprasecca, C. Curutchet, and B. Mennucci, *J. Chem. Theory Comput.*, 2012, **8**, 4462–4473.

25. A. S. Davydov, *Theory of Molecular Excitons*, Plenum, New York, 1971.

26. J. Tomasi, B. Mennucci, and R. Cammi, *Chem. Rev.*, 2005, **105**, 2999–3093.

27. G. Scalmani, M. J. Frisch, B. Mennucci, J. Tomasi, R. Cammi, and V. Barone, *J. Chem. Phys.*, 2006, **124**, 094107-15.

28. T. Forster, *Naturwissenschaften*, 1946, **33**, 166–175.

29. A. Muñoz-Losa, C. Curutchet, B. P. Krueger, L. R. Hartsell, and B. Mennucci, *Biophys. J.*, 2009, **96**, 4779–88.

30. G. Pescitelli, S. Gabriel, Y. Wang, J. Fleischhauer, R. W. Woody, and N. Berova, *J. Am. Chem. Soc.*, 2003, **125**, 7613–28.

31. B. Bosnich, *Acc. Chem. Res.*, 1969, **2**, 266–273.

32. M. H. Koolhaas, G. van der Zwan, F. van Mourik, and R. van Grondelle, *Biophys. J.*, 1997, **72**, 1828–41.

33. M. J. Frisch, G. W. Trucks, H. B. Schlegel, G. E. Scuseria, M. A. Robb, J. R. Cheeseman, G. Scalmani, V. Barone, B. Mennucci, G. A. Petersson, H. Nakatsuji, M. Caricato, X. Li, H. P. Hratchian, A. F. Izmaylov, J. Bloino, G. Zheng, J. L. Sonnenberg, M. Hada, M. Ehara, K. Toyota, R. Fukuda, J. Hasegawa, M. Ishida, T. Nakajima, Y. Honda, O. Kitao, H. Nakai, T. Vreven, J. Montgomery, J. A., J. E. Peralta, F. Ogliaro, M. Bearpark, J. J. Heyd, E. Brothers, K. N. Kudin, V. N. Staroverov, R. Kobayashi, J. Normand, K. Raghavachari, A. Rendell, J. C. Burant, S. S. Iyengar, J. Tomasi, M. Cossi, N. Rega, N. J. Millam, M. Klene, J. E. Knox, J. B. Cross, V. Bakken, C. Adamo, J. Jaramillo, R. Gomperts, R. E. Stratmann, O. Yazyev, A. J. Austin, R. Cammi, C. Pomelli, J. W. Ochterski, R. L. Martin, K. Morokuma, V. G. Zakrzewski, G. A. Voth, P. Salvador, J. J. Dannenberg, S. Dapprich, A. D. Daniels, Ö. Farkas, J. B. Foresman, J. V. Ortiz, J. Cioslowski, and D. J. Fox, Gaussian09, Revision D01; Gaussian, Inc., Wallingford CT; 2009.

34. S. Jurinovich, EXAT - EXcitonic Analysis Tool, 2013, https://www.dcci.unipi.it/molecolab/tools.

35. Y. Zhao and D. G. Truhlar, *Acc. Chem. Res.*, 2008, **41**, 157–67.

36. T. Yanai, D. P. Tew, and N. C. Handy, *Chem. Phys. Lett.*, 2004, **393**, 51–57.

37. R. Fukuda and H. Nakatsuji, *J. Chem. Phys.*, 2008, **128**, 094105-14.

38. U. C. Singh and P. A. Kollman, *J. Comput. Chem.*, 1984, **5**, 129–145.

39. B. H. Besler, K. M. Merz, and P. A. Kollman, *J. Comput. Chem.*, 1990, **11**, 431–439.

40. P. T. van Duijnen and M. Swart, *J. Phys. Chem. A*, 1998, **102**, 2399–2407.

41. A. Shockravi, A. Javadi, and E. Abouzari-Lotf, *RSC Adv.*, 2013, **3**, 6717.

42. J. M. Brunel, *Chem. Rev.*, 2005, **105**, 857–97.

43. L. Meca, D. Reha, and Z. Havlas, *J. Org. Chem.*, 2003, **68**, 5677–80.

44. S. F. Mason, R. H. Seal, and D. R. Roberts, *Tetrahedron*, 1974, **30**, 1671–1682.

45. L. Di Bari, G. Pescitelli, and P. Salvadori, *J. Am. Chem. Soc.*, 1999, **121**, 7998–8004.

46. C. Rosini, S. Superchi, H. W. I. Peerlings, and E. W. Meijer, *Eur. J. Org. Chem.*, 2000, **2000**, 61–71.

47. L. Di Bari, G. Pescitelli, F. Marchetti, and P. Salvadori, *J. Am. Chem. Soc.*, 2000, **122**, 6395–6398.

48. M. Nishizaka, T. Mori, and Y. Inoue, *J. Phys. Chem. A*, 2011, **115**, 5488–95.

49. T. Mori, Y. Inoue, and S. Grimme, *J. Phys. Chem. A*, 2007, **111**, 4222–4234.

50. M. Rubio, M. Merchán, E. Ortí, and B. O. Roos, *Chem. Phys.*, 1994, **179**, 395–409.

51. J. R. Platt, *J. Chem. Phys.*, 1949, **17**, 484-495.

52. H. B. Klevens and J. R. Platt, *J. Chem. Phys.*, 1949, **17**, 470-484.

53. R. A. Singh and S. N. Thakur, *J. Cryst. Mol. Struct.*, 1981, **11**, 197–201.

54. H. Baba and S. Suzuki, *Bull. Chem. Soc. Jpn.*, 1961, **34**, 82–88.

55. K. Nishimoto, *J. Phys. Chem.*, 1963, **67**, 1443–1446.

56. L. S. Forster and K. Nishimoto, *J. Am. Chem. Soc.*, 1965, **87**, 1459–1463.

57. I. Hanazaki and H. Akimoto, *J. Am. Chem. Soc.*, 1972, **94**, 4102–4106.

58. H. Sasai, T. Suzuki, S. Arai, T. Arai, and M. Shibasaki, *J. Am. Chem. Soc.*, 1992, **114**, 4418–4420.

59. A. J. Wooten, P. J. Carroll, and P. J. Walsh, *J. Am. Chem. Soc.*, 2008, **130**, 7407–19.

60. L. Di Bari, M. Lelli, G. Pintacuda, G. Pescitelli, F. Marchetti, and P. Salvadori, *J. Am. Chem. Soc.*, 2003, **125**, 5549–58.

61. L. Di Bari, M. Lelli, G. Pintacuda, G. Pescitelli, F. Marchetti, and P. Salvadori, *J. Am. Chem. Soc.*, 2003, **125**, 5549–58.

62. L. Di Bari, S. Di Pietro, G. Pescitelli, F. Tur, J. Mansilla, and J. M. Saá, *Chem. Eur. J.*, 2010, **16**, 14190–201.